JAST
Journal of Aerospace Science and Technology

Pages: 114-123 / Vol. 16/ Issue 2 / Summer- Fall 2023

Journal of Aerospace Science and Technology

www:jast.ias.ir

Scientific-Research Article

Optimal Round Trip Path-Planning of An Aerial Robot by Consideration of Geometric Constraints of Obstacles

Shayan Dehkhoda[1], **M.A. Amiri Atashgah**[2]*

1- 2- Faculty of New Sciences and Technologies, University of Tehran

ABSTRACT

Keywords: *Optimal path Planning, 6DOF Dynamics, Direct Collocation, Quadrotor, Nonlinear Programming Problem (NLP), Delivery of Goods.*

This paper focuses on optimizing the path planning of a quadrotor for delivering goods in a round-trip mission. The quadrotor is modeled using the Newton-Euler method, and the problem is formulated as an optimal control effort problem. The equations are then discretized using the direct collocation method, turning the problem into a nonlinear programming system that can be solved using available optimization methods. This discretization simplifies the derivative values in the equations of motion and transforms the path optimization problem into a standard form nonlinear programming problem (NLP). Instead of obtaining state and control functions, state and control values are obtained at the beginning and endpoints of smaller time intervals. This method is an explicit method for numerically solving differential equations. The research considers fixed cylindrical safe areas around urban obstacles. Extensive simulations demonstrate the effectiveness of this method in satisfying geometric, dynamic, and kinematic constraints.

Introduction

With the expansion of aerial robot applications, forward-looking companies have decided to employ this technology to transport small goods within their sales and distribution systems [1]. Implementing such a strategy not only has less environmental impact but also proves to be highly efficient in terms of cost and delivery time. Extensive research has been conducted in the field of optimal route design using various methods to achieve the best results in terms of accuracy and speed [2]. One of the researched methods in this context involves designing routes based on intelligent algorithms and machine learning; however, achieving reliable and practical results using these approaches is still a subject of discussion.

Another approach involves utilizing traditional gradient-based optimization methods for route optimization. Various algorithms have been presented in route design using gradient-based techniques [3]. One of the gradient-based algorithms, which is based on the fast descent method, has been introduced by Muren [4]. The significant advantage of this method over other three-dimensional algorithms is separating the three-dimensional solution process into solving two vertical and horizontal planes. It is worth mentioning that most of the research carried out using this approach has been focused on spatial route design. Betts and Huffman have carried out a survey on numerical methods for trajectory optimization [5].

1 Msc.
2 Associate Professor (Corresponding Author) Email: * atashgah@ut.ac.ir

10.22034/jast.2023.326735.1112
Submit: 29.01.2022/ Accepted: 31.01.2023
Print ISSN:2345-3648 Online ISSN: 1735-2134

In this study, the Direct Collocation method is employed to generate reference paths for aerial robots to investigate and case studies of round-trip routes. Furthermore, Norsell [6] has derived an optimal multi-stage route with long distances along with radar coverage constraints for an aircraft. In this approach, the three-dimensional aircraft model has been simplified under various conditions, such as constant altitude flight and other conditions. The desired cost function in this reference is the least detectability by the radar station. Herman and Spencer [7] employed the Direct Collocation method to solve orbital transfer problems, including transfers from low Earth orbits to geostationary, intermediate, and high orbits while considering the minimum fuel cost function. In this reference, the results obtained from the numerical solution method for optimal route design have been compared with results obtained from analytical solution methods. Comparisons indicate that the solutions obtained through the numerical method closely match the analytical approach. Horie and Kanoui [8] used the Direct Collocation method in the context of orbital transfer for a spacecraft to minimize both time and fuel consumption. Furthermore, Moon and Kim [9] proposed a three-dimensional route design method for generating flight paths through sequential passage of several waypoints. However, the passage times through these waypoints in their route model are unspecified; therefore, they introduced an auxiliary variable to account for the unspecified entry times at waypoints.

Lin and Tsai [10] presented a combination of mid-course correction and terminal guidance laws for missile tracking problems. In the successive research stages, Rao [11] enhanced the analytical solutions by accounting for nonlinear terms that were previously neglected by Lin and Tsai. Additionally, Shippey utilized a Direct Collocation method and non-linear programming based on a combination of genetic algorithms and direct shooting methods to solve optimal control problems [12]. It is worth mentioning that one of the effective sources in the field of optimal control and the use of the Direct Collocation method in aerial robots for goods delivery is [13]. This source served as the initial foundation for the current research, and by making modifications to the solver framework and customizing the number of nodes for round-trip missions, the feasibility of the proposed idea is being investigated. In summary, for those readers interested in pursuing further research, it is advisable to delve into the investigations outlined in references [14] through [17].

It is noteworthy that the majority of endeavors, in accordance with the referenced citations, have been concentrated on applying optimal route design methodologies. Researchers remain engaged in feasibility studies and case analyses, aiming to leverage existing machine learning approaches for constructing comprehensive training datasets. It is vital to emphasize that the research presented herein is profoundly pragmatic in nature. The practical deployment of quadcopter drones for cargo delivery and related research subjects continues to captivate scholarly interest. A significant point of discourse in the practical implementation of these aerial robots revolves around the intricate, fully nonlinear dynamics inherent to these drones. This complexity renders the design of a robust path and controller a nontrivial undertaking. In realizing the proposed concept, this research employs a dynamic model encompassing 12 state, four input, and four output variables, thereby encapsulating the intricate dynamics and relevant constraints underpinning this study. Another groundbreaking facet is incorporating a round-trip path design, wherein the drone undertakes the journey to retrieve the cargo, transports it to its destination, and returns. Along this trajectory, while adhering to mission time constraints, the drone strives to minimize control efforts to conserve energy consumption.

Subsequent to this point, the article unfolds across sections two to five, wherein comprehensive insights into modeling intricacies, optimization procedures, and resultant outcomes are meticulously delineated.

The Dynamic Model of Quadcopter

As depicted in Figure (1), the control and stability of a quadcopter aerial robot inherently involve the manipulation of motor speeds. Due to its six degrees of freedom and being controlled by four actuators, this device is an underactuated system. The six degrees of freedom encompass three translational movements along the *x, y, and z* axes and three rotational movements-roll, pitch, and yaw [18]. Typically, to analyze the motion of a rigid body with six degrees of freedom, two coordinate systems, namely the inertial/navigation (*n*) and body (*b*) frames, are employed .

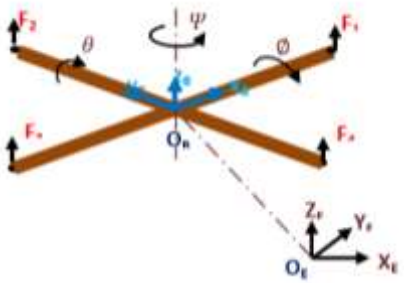

Figure 1 Angular Motion [19].

Finally, the vector of the state variables of the robot can be expressed as follows.

$$\boldsymbol{x} = [x \quad y \quad z \quad \dot{x} \quad \dot{y} \quad \dot{z} \quad \phi \quad \theta \quad \psi \quad \dot{\phi} \quad \dot{\theta} \quad \dot{\psi}] \tag{1}$$

The position $\Gamma^n = [x\ y\ z]^{\mathrm{T}}$ and attitude $\Theta^n = [\phi\ \ \theta\ \ \psi]^T$ vectors in the navigation system, as well as the translational velocity $V^b = [\mathrm{u\ v\ w}]^{\mathrm{T}}$ and rotational velocity $\omega^b = [\mathrm{p\ q\ r}]^{\mathrm{T}}$ vectors in the physical body, are formed using the components of the state vectors. For transferring the translational velocities from the physical body to the inertia, one can write:

$$\begin{bmatrix} \dot{x} \\ \dot{y} \\ \dot{z} \end{bmatrix} = \mathbf{R}(\psi, \mathrm{z}^n)\mathbf{R}(\theta, \mathrm{y}^{(2)})\mathbf{R}(\phi, \mathrm{x}^b) \begin{bmatrix} u \\ v \\ w \end{bmatrix} = \mathbf{R}_{\Theta} \begin{bmatrix} u \\ v \\ w \end{bmatrix} \tag{2}$$

In order to transfer rotational velocities from the body to the inertia frame, the following relation can be used:

$$\begin{bmatrix} \dot{\phi} \\ \dot{\theta} \\ \dot{\psi} \end{bmatrix} = \begin{bmatrix} p \\ 0 \\ 0 \end{bmatrix} + \mathbf{R}(\phi, \mathrm{x}^b) \begin{bmatrix} 0 \\ q \\ 0 \end{bmatrix} + \mathbf{R}(\theta, \mathrm{y}^{(2)})\mathbf{R}(\phi, \mathrm{x}^b) \begin{bmatrix} 0 \\ 0 \\ r \end{bmatrix}$$

$$= \mathbf{T}_{\Theta} \begin{bmatrix} p \\ q \\ r \end{bmatrix} = \begin{bmatrix} 1 & \sin\phi\tan\theta & \cos\phi\tan\theta \\ 0 & \cos\phi & -\sin\phi \\ 0 & \dfrac{\sin\phi}{\cos\theta} & \dfrac{\cos\phi}{\cos\theta} \end{bmatrix} \begin{bmatrix} p \\ q \\ r \end{bmatrix} \tag{3}$$

The development of dynamic equations for an aerial robot using the Newton-Euler method has been performed. The resulting equations are nonlinear, under-actuated, and possess inherent dynamic instability. This implies that when the robot deviates from equilibrium due to environmental disturbances, it will practically not return to equilibrium without applying control inputs [18]. The aerodynamic forces resulting from rotor rotations are proportional to the rotor's angular velocity squared. Furthermore, the aerodynamic forces and torques acting on the quadcopter are modeled as follows.

$$\begin{aligned} U_1 &= b(\Omega_1^2 + \Omega_2^2 + \Omega_3^2 + \Omega_4^2) \\ U_2 &= bl(-\Omega_2^2 + \Omega_4^2) \\ U_3 &= bl(\Omega_1^2 - \Omega_3^2) \\ U_4 &= d(\Omega_1^2 - \Omega_2^2 + \Omega_3^2 - \Omega_4^2) \end{aligned} \tag{4}$$

In which U_1 the upward force, U_2 the torque about x^b , U_3 the torque about y^b, and U_4 the torque about z^b. Additionally, it includes b the coefficient of system propulsion, ι the length of the quadcopter arm, and d the coefficient of drag. Other aerodynamic effects, such as the angle of attack, blade deflection, and airflow turbulence at reference points, have also been examined [18]; however, due to the complexity of modeling these effects and their significant impact only at high speeds, they are disregarded from being included in the quadcopter model. According to Newton's second law, the translational dynamic equations of a rigid body are as follows:

$$\mathrm{m}\ddot{\mathbf{\Gamma}} = \mathbf{F}^n \tag{5}$$

In which m the mass of the quadcopter and $\mathbf{F}^n$ the total forces applied to it are in the reference frame (navigation frame). The translational motion equations are based on Newton's laws in the body-fixed frame and are represented by equations (6) to (8); the parameters present are weight, propeller thrust forces, and aerodynamic forces acting on the robot's body system.

$$\begin{bmatrix} \dot{u} \\ \dot{v} \\ \dot{w} \end{bmatrix} = \begin{bmatrix} rv - qw - g\sin\theta \\ -ru + pw + g\sin\phi\cos\theta \\ qu - pv + g\cos\theta\cos\phi + \dfrac{U_1}{m} \end{bmatrix} \tag{6}$$

$$\mathrm{m}\ddot{\mathbf{\Gamma}} = \mathbf{R}_{\Theta} \begin{bmatrix} 0 \\ 0 \\ -U_1 \end{bmatrix} + \begin{bmatrix} 0 \\ 0 \\ mg \end{bmatrix} \tag{7}$$

$$= \frac{-U_1}{m}[\cos\psi \sin\theta \cos\phi + \sin\psi \sin\phi]$$
$$= \frac{-U_1}{m}[\sin\psi \sin\theta \cos\phi - \cos\psi \sin\phi] \quad (8)$$
$$= g - \frac{U_1 \cos\phi \cos\theta}{m}$$

Furthermore, utilizing Euler's theorem, the equation of rotational dynamics is expressed in the following:

$$\mathbf{I}\dot{\boldsymbol{\omega}} + \boldsymbol{\omega} \times (\mathbf{I}\boldsymbol{\omega}) = \boldsymbol{\tau}^b \quad (9)$$

The main factor causing angular accelerations in rotational motion equations is the external torques applied to the flying robot. The final equations of rotational motion in the body frame will be calculated by calculating the individual external torques applied [18].

$$\dot{p} = qr\left(\frac{I_{yy} - I_{zz}}{I_{xx}}\right) + \frac{J_r q \Omega_r}{I_{xx}} + \frac{U_2}{I_{xx}}$$
$$\dot{q} = pr\left(\frac{I_{zz} - I_{xx}}{I_{yy}}\right) - \frac{J_r p \Omega_r}{I_{yy}} + \frac{U_3}{I_{yy}} \quad (10)$$
$$\dot{r} = qp\left(\frac{I_{xx} - I_{yy}}{I_{zz}}\right) + \frac{U_4}{I_{zz}}$$

In which Ω_r is the result of the rotor angular velocity and $J_r$stands for the rotor's moment of inertia. The rotational dynamic equations can also be obtained in terms of Euler angles [19].

$$\begin{bmatrix} \ddot{\phi} \\ \ddot{\theta} \\ \ddot{\psi} \end{bmatrix} = \frac{d(\mathbf{T}_\Theta \boldsymbol{\omega})}{dt} = \dot{\mathbf{T}}_\Theta \boldsymbol{\omega} + \mathbf{T}_\Theta \dot{\boldsymbol{\omega}} \quad (11)$$

Optimal 6DoF Path Design

In the process of route design, which takes place before a flight, mathematical solutions based on optimization methods are often used. These methods usually possess a nature that is dependent on and sensitive to the boundary conditions of the problem. Route design is consistently divided into two parts: the first part is non-sequential, while the second part is sequential; in other words, the primary focus in the first part is on designing the route, and in the second part, it involves controlling the route. In path optimization problems, in order to generate an optimal route, fulfilling the dynamic and functional constraints of the vehicle is necessary.

In each path optimization problem, a set of dynamic equations are presented to describe the governing equations of the dynamic process. These equations allow the system's state to be obtained for control input values at any given moment. This set of equations is generally expressed in the state space and referred to as state equations [20],[21].

$$\dot{\mathbf{x}} = \mathbf{f}(\mathbf{x}(t), \mathbf{u}(t), t) \quad (12)$$

Each path optimization problem involves multiple state variables (**x**) to describe the system's state at each moment and multiple control variables (**u**) to exert control over the system at each moment. In the equation above, *t* represents time, and **f** is a vector of nonlinear functions. In this context, the governing equations refer to the aggregation of dynamic and kinematic equations mentioned in the previous section, considering 12 state variables, 4 input variables, and 4 output variables.

Path optimization problems are defined within a time interval, where the starting moment of this interval (t_0) is usually specified. Still, the final time of this interval (t_f) can be fixed or free. In other words, path optimization problems are solved in certain cases within a specific time interval and in other cases within an unspecified time interval.

$$t \in [t_0, t_f] \quad (13)$$

In path optimization problems, various constraints are determined and defined based on the vehicle's limitations, environmental constraints, or the desired conditions of path designers. These constraints are generally divided into two categories: point constraints and path constraints. Point constraints are applied to the problem at specific and distinct time instances. Constraints related to initial conditions (ψ_0) and final conditions of the problem (ψ_f), defined at the start and end moments of the path, are considered point constraints. These constraints can involve explicit and specific values of state variables or be expressed as functions of these variables.

In some path optimization problems, point constraints are defined at intermediate points (intermediate times).

$$\Psi_0(\mathbf{x}(t_0), t_0) \geq 0 \quad (14)$$

$$\Psi_f(\mathbf{x}(t_f), t_f) \geq 0 \quad (15)$$

However, path constraints (**g**) are constraints that are applied to the problem over a time interval, which

can encompass either the entire or a portion of the problem's time span [20],[21].

$$\mathbf{g}(\mathbf{x}(t),\mathbf{u}(t),t)\geq\mathbf{0} \tag{16}$$

In path optimization problems, it's possible to define bounds on the range of variations for state and control variables within a specific interval; this means setting upper and lower limits for each variable. Boundaries for state variables can be established based on physical constraints or the goals of the designers. Boundaries for control variables are defined based on the limitations of control components.

$$\mathbf{x}_l \leq \mathbf{x}(t) \leq \mathbf{x}_u \tag{17}$$

$$\mathbf{u}_l \leq \mathbf{u}(t) \leq \mathbf{u}_u \tag{18}$$

In general, all the constraints considered in this study and their corresponding initial conditions are notable in Table (2). In each optimization problem, the main objective is to achieve a set of optimal control inputs while satisfying constraints and minimizing the cost function. This optimization event is expressed as a scalar objective function or performance criterion *J*, typically formulated as follows, and needs to be minimized:

$$J=\phi\left(\mathbf{x}\left(t_f\right),t_f\right)+\int_{t_0}^{t_f} L\left(\mathbf{x}(t),\mathbf{u}(t),t\right)dt \tag{19}$$

This parameter consists of two parts: the pointwise final value constraints (ϕ) and the integral/Lagrangian path constraint (L). Path optimization problems can be expressed in a multi-stage manner, where the time interval of the problem is composed of the combination of several smaller consecutive time intervals. Each of these sub-intervals can be treated as an independent optimization problem. However, there are connections between state and control variables across these time phases, at the beginning and end of each phase, which lead to the integration of the overall problem. The time intervals of these phases can be fixed or free. Subsequently, the process of solving the optimization problem based on a Direct Collocation method is presented.

Direct Collocation Method

The Direct Collocation method is a technique used in path optimization problems to solve the optimization process in a stepwise manner. In this approach, the overall optimization problem is divided into smaller sub-problems, often referred to as phases. These phases correspond to consecutive time intervals within the entire trajectory.

Each phase is treated as an independent optimization problem where the objective is to find optimal control inputs that satisfy constraints and minimize the cost function for that specific phase. The optimization process proceeds sequentially through these phases, considering the relationships and continuity between state and control variables at the boundaries of each phase.

The direct sequential method allows for a systematic approach to solving complex path optimization problems by breaking them down into manageable parts. The connection between consecutive phases ensures the overall coherence of the solution. This method also provides flexibility in terms of defining fixed or free time intervals for each phase, depending on the specific characteristics of the problem.

Overall, the direct sequential method simplifies the optimization process by tackling smaller sub-problems one after another, ultimately leading to an optimized trajectory that adheres to constraints and minimizes the cost function.

By employing these numerical integration methods, the differential and integral expressions of the path optimization problem are transformed into simple algebraic equations ζ_k in terms of discrete state and control variables at time nodes. In other words, to discretize the state equations in a general form, numerical integration methods like Hermite-Simpson (Equation 20) can be utilized, where h_k represents the time interval between two consecutive nodes [14]-[17] .

$$\begin{gathered}\zeta_k = x_{k+1} - x_k - \frac{h_k}{6}\left(f_k + 4\bar{f}_{k+1} + f_{k+1}\right) = 0 \\ \bar{f}_{k+1} = f\left(\bar{x}_{k+1}, \bar{u}_{k+1}, t_k + \frac{h_k}{2}\right) \\ \bar{x}_{k+1} = \frac{1}{2}(x_k + x_{k+1}) + \frac{h_k}{8}(f_k - f_{k+1}) \\ \bar{u}_{k+1} = \frac{1}{2}(u_k + u_{k+1})\end{gathered} \tag{20}$$

As evident, using numerical integration methods transforms the state equations into algebraic equality constraints. Based on this, equality constraints must be created for the number of time sub-intervals to enforce a state equation. Suppose there are path constraints in the optimization problem. In that case, these constraints can also be defined at each time node using the discrete optimization variables defined for that time node and applied to the optimization problem.

In the case of a free final time in the optimization problem, the final time itself is considered an optimization variable.

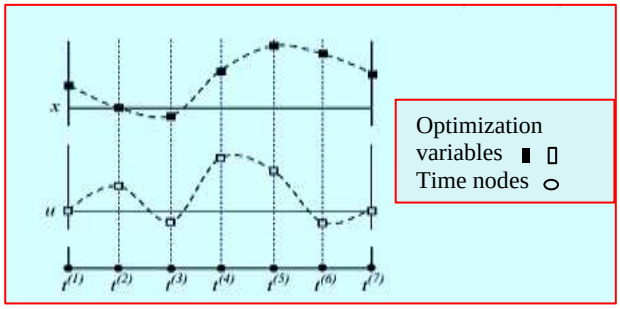

Figure 2. The process of discretization [13].

Geometric Model of Obstacles

In this study, a cylinder with a specified radius and center position has been utilized for modeling the safe margins around each of the structures along the path. The generated path is designed to avoid passing through the interior of any of these cylinders. To achieve this, the distance of each time node from the path to the center of each cylinder is calculated, and this distance is incorporated as an inequality constraint to ensure it is larger than the radius of that cylinder. It's worth noting that a margin of 10% of the obstacle radius is considered in the applied inequality constraints. The reasons for employing this margin are as follows:[۱۹]

The employed aerial robot in this study has dimensions of about one meter. Therefore, the distance of each time node to the center of obstacles should be slightly larger than the obstacle radius to prevent the aerial robot from colliding with the obstacles.

In case the aerial robot encounters a failure during maneuvering, it should be able to continue its path without colliding with obstacles.

It's important to mention that the study uses 7 cylindrical obstacles with radii of 8, 10, 14, 14, 9, 13, and 10 meters, all with a height of 25 meters. These radii are determined based on the environmental radius of each structure. A final height constraint of 18 meters is also applied to the aerial robot's path. The reasons for this constraint are as follows:

- Since the defined mission for the aerial robot is good delivery, this study aims to have the robot fly as low as possible.

- Considering that the defined mission for the aerial robot takes place within an urban environment, the desire is for the robot to fly over the top of the existing structures along the flight path to preserve the privacy of these buildings.

Solver and Solution Method

Due to its inherently numerical nature, nonlinear programming is highly suitable for research in algorithmic and software-related fields. Currently, various open-source packages are available under the title of nonlinear programming solvers. These packages enable path optimization designers to focus solely on transforming path optimization problems into nonlinear programming problems. One of these solvers is the open-source package "IPOPT" [21]. This package employs the Dual Interior-point Algorithm for solving nonlinear programming problems. The IPOPT software includes dozens of subroutines in Fortran and C++, which, when combined, can solve large-scale nonlinear programming problems [22].

Results and Analysis

This section presents the results obtained from simulation and optimal problem-solving for the constrained optimal 3D path planning (with 6 degrees of freedom) in a round-trip flight for the desired aerial robot. It is important to note that the forward path consists of 20 nodes, and the return path also comprises 20 nodes. As observed, the direct sequential method has successfully generated the desired round-trip path while adhering to equality and inequality constraints, avoiding obstacles, and minimizing control effort. Furthermore, the specifications of the utilized aerial robot can be found in Table 1.

Table 1. Physical Characteristics of Flying Robot [13].

Characteristic	Value and Symbol
mass	$m=0.52(kg)$
Length of each arm	$l=0.232(m)$
Constant Trust Coefficient	$b=3.13*10^{-5}(N.s^2)$
Fixed drag coefficient	$d=7.5*10^{-7}(N.m.s^2)$
Body Inertia Moment around the x axis	$I_x=6.228*10^{-3}(Kg.m^2)$
Body Inertia Moment around the y axis	$I_y=6.225*10^{-3}(Kg.m^2)$
Body Inertia Moment around the z axis	$I_z=1.121*10^{-2}(Kg.m^2)$
Moment of inertia of each motor around the z axis	$I_R=6*10^{-5}(Kg.m^2)$

Furthermore, the initial and final conditions employed in the path design using the direct collocation method, which is utilized in this study,

are presented in Table (2). It's worth mentioning that operational conditions provided by [13] have been adopted for the purpose of result validation.

Table 1. Initial and Final Conditions of the Route

Parameter	Beginning and Final Mission Conditions	Intermediate Conditions (Delivery)
$t\ (s)$	140	-
$\emptyset\ (deg)$	0	**0**
$\dot{\emptyset}\ (deg)$	0	**0/3**
$\theta\ (deg)$	0	**0/3**
$\dot{\theta}\ (deg)$	0	**0/3**
$\psi\ (deg)$	0	**0/3**
$\dot{\psi}\ (deg)$	0	**0/3**
$x\ (m)$	0	**300**
$\dot{x}\ (m/s)$	1	**1**
$y\ (m)$	200	**250**
$\dot{y}\ (m/s)$	0	**0/1**
$z\ (m)$	1	**18**
$\dot{z}\ (m/s)$	0	**0/1**

It should be noted that Figure (3) depicts the top view of the path, and Figure (4) presents the three-dimensional view of the path, where the aerial robot successfully traverses the path without colliding with obstacles. As can be observed, the direct collocation method has effectively solved this constrained optimal control problem, considering all the constraints, ensuring collision avoidance, and minimizing control effort. The blue path represents the forward path, and the red path represents the return path. Additionally, Figures (5) to (8) display the control effort of each rotor along the x-axis, with the green path denoting the forward path and the red path indicating the return path in the negative direction. Path design has aimed to minimize these control effort signals. Now, moving on to the analysis of changes in Cartesian velocities along the path, illustrated in Figures (9) to (11). In Figure (9), the x-velocity is depicted. The horizontal axis represents the quadrotor's position along the path from start to the end of the good delivery mission and its return. According to the graph, the x-velocity changes between 1 to 4 meters per second. Continuing with Figure (10), it shows the y-velocity. The horizontal axis still represents the quadrotor's position along the path. The y-velocity ranges from -2 to -2.5 meters per second, indicating the solver's ability to satisfy dynamic constraints. Finally, Figure (11) displays the z-velocity. Once again, the horizontal axis indicates the quadrotor's position along the path. The z-velocity changes between 0.1 to 0.15 meters per second, demonstrating the accuracy of the solver's output in adhering to the dynamic constraints. Considering the previous observations, the cost function graph in Figure (12), executed for around 800 thousand iterations, indicates that despite satisfying all the constraints, the cost function continues to oscillate around its minimum value after 5000 iterations.

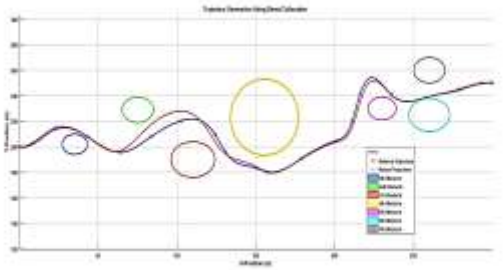

Figure 3. The top of the 3D path.

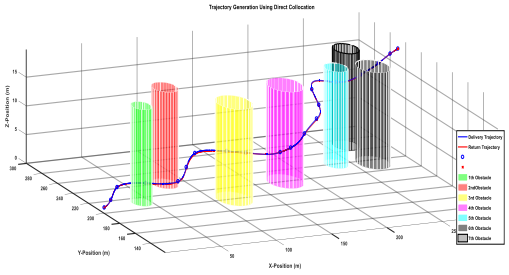

Figure 4. 3D view of the path.

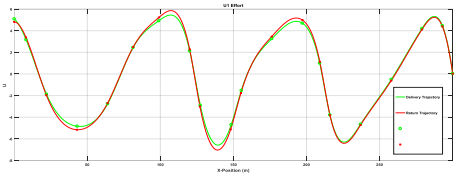

Figure 5. Rotor 1 Control Effort.

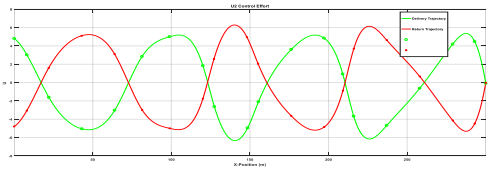

Figure 6. Rotor 2 Control Effort.

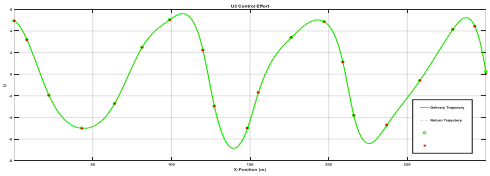

Figure 7. Rotor 3 Control Effort.

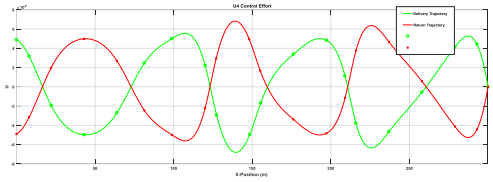

Figure 8. Rotor 4 Control Effort.

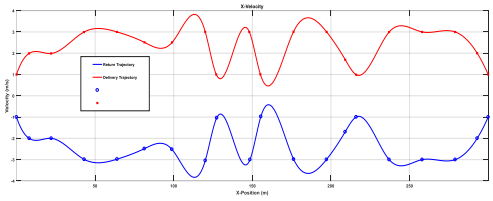

Figure 9. X Linear Velicity.

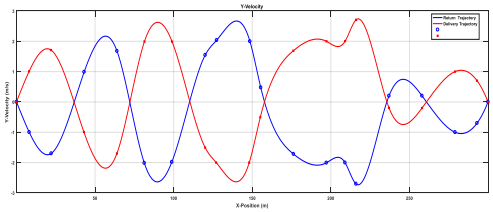

Figure 10. Y Linear Velicity.

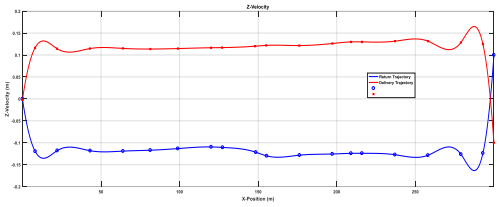

Figure 11. Z Linear Velicity.

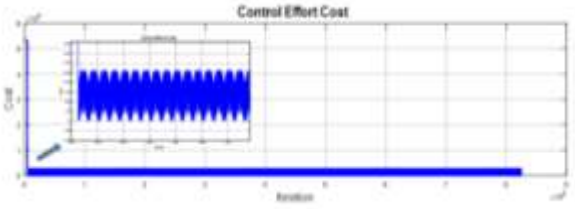

Figure 12. Cost of the control effort vs. the number of Iterations.

Given the obtained velocity values, it can be inferred that the practical implementation and deployment of the proposed method, ensuring the safe delivery of cargo to its destination, are feasible. However, by making necessary changes to the problem constraints, this method can be extended for various types of cargo delivery missions and for utilization with diverse aerial vehicles. It's important to note that while there isn't a significant difference in the control inputs for the first and third dimensions, noticeable differences are present in the control inputs for the second and fourth dimensions. This is due to the nature of the delivery mission involving both outbound and return paths. In order to accommodate height changes in the opposite direction while simultaneously maintaining balance in both the longitudinal and lateral aspects of the aerial robot, distinct solutions were effectively obtained for the return path in these specified control channels.

Conclusions

The main objective of this research was to design and follow an optimal constrained three-dimensional path for a six-degree-of-freedom quadcopter for cargo/goods delivery. Simulation results for the optimal constrained three-dimensional path design were presented. In other words, considering the dynamics of the aerial robot and the defined mission, a flight path for cargo delivery was designed in a way that satisfies geometric constraints along the path, specifically urban constraints related to buildings. Furthermore, the cost function employed in this study aimed to minimize the control effort required for flight. Ultimately, it was observed that by utilizing the direct sequencing method, all constraints were satisfied, maintaining a safe distance from obstacles, and an optimal three-dimensional path for cargo delivery was generated with minimal control effort. Moving forward, the enhancement of the proposed method could involve integrating path design techniques with intelligent approaches for further optimization.

References

[1] A. Mohammadi, E. Abbasi, M. Ghayour, and M. Danesh, “Formation Control and Path Tracking for a Group of Quadrotors to Carry Out a Suspended Load,” *Modarres Mechanical Engineering*, vol. 19, no. 4, 2019.

[2] Li Qing, “Aircraft route optimization using genetic algorithms,” pp. 394–397, 2005, doi: 10.1049/cp:19971212.

[3] L. Yang, J. Qi, D. Song, J. Xiao, J. Han, and Y. Xia, “Survey of robot 3D path planning algorithms,” *Journal of Control Science and Engineering*, vol. 2016, 2016.

[4] Muren, J. Wu, L. Zhou, Z. Du, and Y. Lv, “Mixed steepest descent algorithm for the traveling salesman problem and application in air logistics,” *Transportation Research Part E: Logistics and Transportation Review*, vol. 126, pp. 87–102, Jun. 2019, doi: 10.1016/j.tre.2019.04.004.

[5] J. T. Betts, “Survey of numerical methods for trajectory optimization,” *Journal of guidance, control, and dynamics*, vol. 21, no. 2, pp. 193–207, 1998.

[6] M. Norsell, “Multistage trajectory optimization with radar range constraints,” *Journal of aircraft*, vol. 42, no. 4, pp. 849–857, 2005.

[7] A. L. Herman and D. B. Spencer, “Optimal, low-thrust earth-orbit transfers using higher-order collocation methods,” *Journal of Guidance, Control, and Dynamics*, vol. 25, no. 1, pp. 40–47, 2002.

[8] K. Horie and B. A. Conway, "Optimal aeroassisted orbital interception," *Journal of guidance, control, and dynamics*, vol. 22, no. 5, pp. 625–631, 1999.

[9] G. Moon and Y. Kim, "Flight path optimization passing through waypoints for autonomous flight control systems," *Engineering Optimization*, vol. 37, no. 7, pp. 755–774, 2005.

[10] C. F. Lin and L. L. Tsai, "Analytical solution of optimal trajectory-shaping guidance," *Journal of Guidance, Control, and Dynamics*, vol. 10, no. 1, pp. 60–66, Jan. 1987, doi: 10.2514/3.20181.

[11] M. N. Rao, "Analytical solution of optimal trajectory-shaping guidance," *Journal of Guidance, Control, and Dynamics*, vol. 12, no. 4, pp. 600–601, Jul. 1989, doi: 10.2514/3.20451.

[12] B. M. Shippey, "Trajectory optimization using collocation and evolutionary programming for constrained nonlinear dynamical systems," The University of Texas at Arlington, 2008.

[13] A. L. Yanesi, "Three-Dimensional Constrained Optimal Motion Planning and its Robust Tracking Control Design for a Six-Degree-of-Freedom Quadrotor-Helicopter for Urban Traffic Purposes," Tehran, 2014.

[14] R. Bordalba, T. Schoels, L. Ros, J. M. Porta, and M. Diehl, "Direct Collocation Methods for Trajectory Optimization in Constrained Robotic Systems," *IEEE Transactions on Robotics*, pp. 1–20, 2022, doi: 10.1109/TRO.2022.3193776.

[15] A. Angelopoulos *et al.*, "Drone Brush: Mixed Reality Drone Path Planning," in *2022 17th ACM/IEEE International Conference on Human-Robot Interaction (HRI)*, Mar. 2022, pp. 678–682. doi: 10.1109/HRI53351.2022.9889504.

[16] M. T. R. Khan, M. Muhammad Saad, Y. Ru, J. Seo, and D. Kim, "Aspects of unmanned aerial vehicles path planning: Overview and applications," *International Journal of Communication Systems*, vol. 34, no. 10, Jul. 2021, doi: 10.1002/dac.4827.

[17] S.-H. Kim, G. E. G. Padilla, K.-J. Kim, and K.-H. Yu, "Flight Path Planning for a Solar Powered UAV in Wind Fields Using Direct Collocation," *IEEE Trans Aerosp Electron Syst*, vol. 56, no. 2, pp. 1094–1105, Apr. 2020, doi: 10.1109/TAES.2019.2926654.

[18] C. Balas, "Modelling and linear control of a quadrotor," *Cranfield University, MSc Thesis*, vol. 2007, 2006.

[19] A. Lavaei and M. A. A. Atashgah, "Optimal 3D trajectory generation in delivering missions under urban constraints for a flying robot," *Intelligent Service Robots*, vol. 10, no. 3, 2017, doi: 10.1007/s11370-017-0225-x.

[20] P. Zarafshan, S. B. Moosavian, S. A. A. Moosavian, and M. Bahrami, "Optimal control of an aerial robot," in *2008 IEEE/ASME International Conference on Advanced Intelligent Mechatronics*, 2008, pp. 1284–1289.

[21] M. Forkan, M. M. Rizvi, and M. A. M. Chowdhury, "Optimal path planning of Unmanned Aerial Vehicles (UAVs) for targets touring: Geometric and arc parameterization approaches," *Plos One*, vol. 17, no. 10, p. e0276105, Oct. 2022, doi: 10.1371/journal.pone.0276105.

[22] K. Chen, D. Zhang, K. Wang, Z. Shao, and L. T. Biegler, "Nonlinear homotopy interior-point algorithm for 6-DoF powered landing guidance," *Aerospace Sci Tech*, vol. 127, p. 107707, Aug. 2022, doi: 10.1016/j.ast.2022.107707.